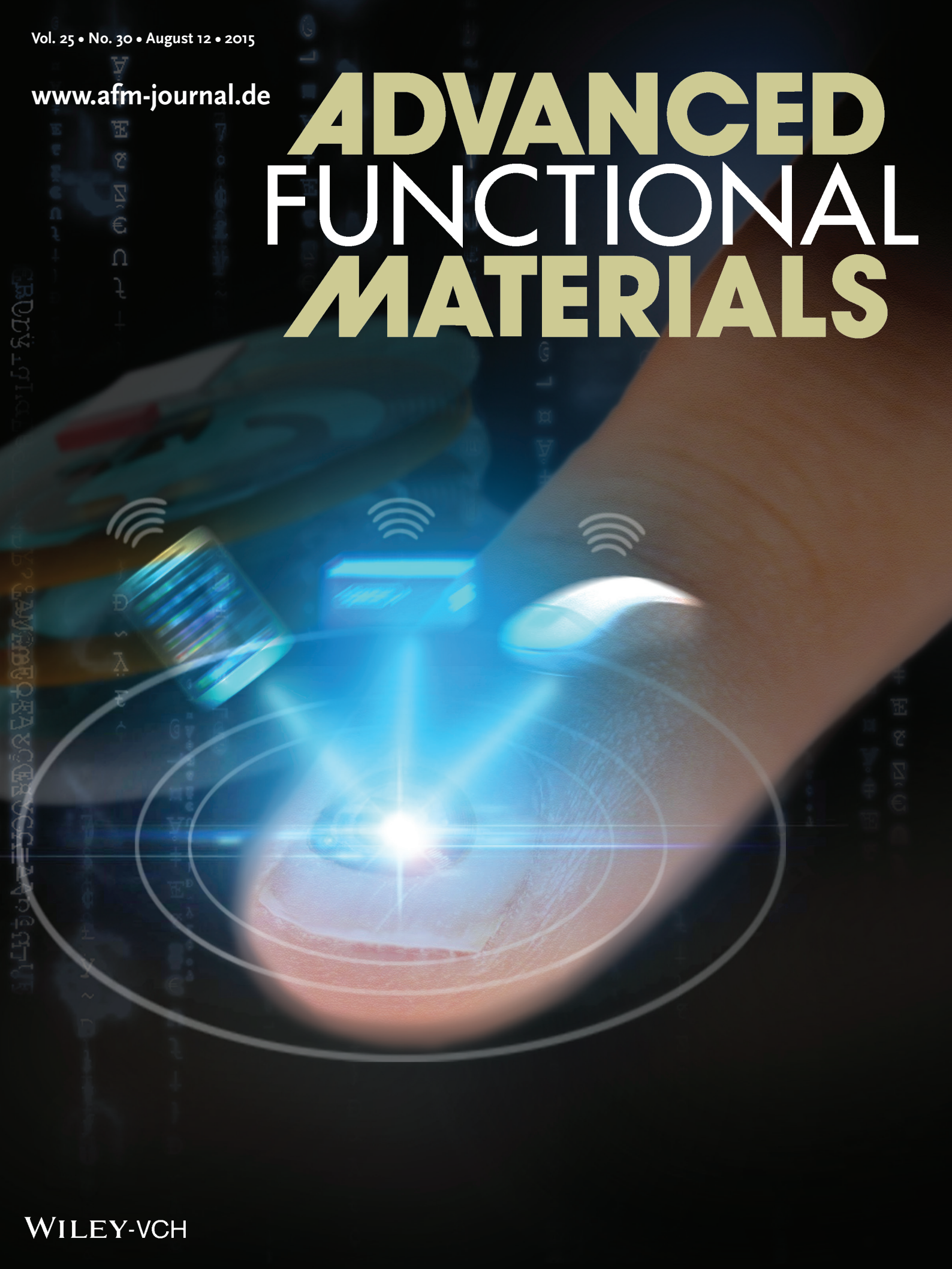


Vol. 25 • No. 30 • August 12 • 2015

www.afm-journal.de

ADVANCED FUNCTIONAL MATERIALS



WILEY-VCH

Miniaturized Flexible Electronic Systems with Wireless Power and Near-Field Communication Capabilities

Jeonghyun Kim, Anthony Banks, Zhaoqian Xie, Seung Yun Heo, Philipp Gutruf, Jung Woo Lee, Sheng Xu, Kyung-In Jang, Fei Liu, Gregory Brown, Junghyun Choi, Joo Hyun Kim, Xue Feng, Yonggang Huang, Ungyu Paik,* and John A. Rogers*

A class of thin, lightweight, flexible, near-field communication (NFC) devices with ultraminiaturized format is introduced, and systematic investigations of the mechanics, radio frequency characteristics, and materials aspects associated with their optimized construction are presented. These systems allow advantages in mechanical strength, placement versatility, and minimized interfacial stresses compared to other NFC technologies and wearable electronics. Detailed experimental studies and theoretical modeling of the mechanical and electromagnetic properties of these systems establish understanding of the key design considerations. These concepts can apply to many other types of wireless communication systems including biosensors and electronic implants.

1. Introduction

Wearable electronic technologies form the foundation for a rapidly growing consumer device segment. Projections suggest that over \$100 billion will be spent in materials alone over the coming decade in the pursuit of new wearable devices.^[1] Advances in materials and device architectures for these systems will create opportunities for increasing the range of capabilities, expanding the modes of use, improving the robustness/reliability, reducing the size/weight, and lowering the cost. The cellular phone platform will likely remain a key element in the broader

technology landscape, as in currently available wrist band and watch style devices that measure body processes and communicate data to the phone.^[2,3] Recent research demonstrates much different types of integration strategies compared to those of these existing systems, in which the wearable devices take the form of temporary transfer tattoos. The result is greatly improved contact with the body and corresponding increases in the diversity and accuracy of information that can be collected from integrated sensors.^[2,4,5] Here, an overarching goal is to engineer the physical properties, and in particular the elastic modulus and elastic stretchability, to match those of the epidermis, as a way to reduce irritation and discomfort at the skin interface and to improve the robustness of the bonding.^[2,4,6] In this paper, we present a complementary strategy, in which overall size miniaturization serves as an additional, and sometimes primary, means for minimizing physical effects on the skin. This scheme also expands the options in mounting locations to include areas such as the fingernails and the teeth, where mechanical compliance is no longer required and where mounting times can extend to several months, or more. In particular, we introduce thin, lightweight, flexible near field communication (NFC) devices in ultraminiaturized formats, along with systematic studies of the mechanics and materials aspects associated with their optimized construction. The potential applications include password authentication,^[7] electronic transactions,^[8] and biometric sensing,^[9] each performed via wireless power and communication to cellular phones or other NFC-enabled platforms. Such devices consume nearly one hundred times less area than conventional wrist-worn NFC devices and they are ≈ 100 and $\approx 10\,000$ times thinner and lighter,

J. Kim, A. Banks, S. Y. Heo, Dr. J. W. Lee, Dr. S. Xu, Dr. K.-I. Jang, G. Brown, Prof. J. A. Rogers
Department of Materials Science and Engineering
Frederick Seitz Materials Research Laboratory
University of Illinois at Urbana-Champaign
Urbana, IL 61801, USA
E-mail: jrogers@illinois.edu



J. Kim, Dr. J. W. Lee, J. Choi, J. H. Kim, Prof. U. Paik
Department of Materials Science and Engineering
Department of Energy Engineering
Hanyang University
Seoul 133-791, Republic of Korea
E-mail: upaik@hanyang.ac.kr

Dr. Z. Xie, Prof. Y. Huang
Department of Mechanical Engineering
Civil and Environmental Engineering
Center for Engineering and Health, and Skin Disease Research Center
Northwestern University
Evanston, IL 60208, USA

Dr. Z. Xie, F. Liu, Prof. X. Feng
AML, Department of Engineering Mechanics
Center for Mechanics and Materials
Tsinghua University
Beijing 100084, China

P. Gutruf
Functional Materials and Microsystems Research Group
School of Electrical and Computer Engineering
RMIT University
Melbourne, VIC 3000, Australia

DOI: 10.1002/adfm.201501590

respectively. The areas are also nearly ten times smaller than those of recently reported NFC devices with epidermal construction^[2] and are, to our knowledge, the smallest to be explored for integration on the surface of the human body. Rigid, capsule-shaped NFC devices with volumes approximately ten times larger than those of the devices reported here are available for implantation into human body.^[10] Open architecture designs provide a high tolerance to deformation and physical stresses when mounted on soft surfaces such as the epidermis. Experimental measurements of the mechanical and electromagnetic properties compare favorably to theoretical modeling results. Device operation using standard NFC-enabled consumer electronics demonstrates the capabilities in evaluations that are suggestive of envisioned applications.

2. Results and Discussion

Figure 1 summarizes the layered, open architecture designs of these ultraminiaturized, or millimeter-scale, NFC (mm-NFC) devices. Figure 1a,b shows optical microscope images of mm-NFC devices with diameters of 5.8 and 7.04 mm. For both cases, each of the coils in the dual-coil layout consists of copper traces with nine turns (18 μm thick) to enable high Q factors and resonance frequencies near 14 MHz (Figure 1c,d). These platforms exploit thinned NFC die selected from a range of commercially available components. The experiments reported here use NTAG216 (NXP Semiconductor) and M24LR04E (ST Microelectronics) chips with the 5.8 and 7.04 mm diameter coils, respectively. The devices incorporate polyimide coatings above and below each layer to physically encapsulate the copper traces and place them near the neutral mechanical plane to minimize bending induced strains (Figure 1d,e). The NFC dies connect via a modified flip-chip technique to contacts located near the center regions of the coils. Certain device variants also include small-scale light-emitting diodes (LEDs, 0402 size: 1 mm \times 0.5 mm). Here, energy harvested and rectified during communication within NFC ISO protocols enables operation of the LEDs and the NFC chips simultaneously. When a smartphone or other NFC reader is sufficiently close, the NFC device is powered automatically and the LED turns on at same time (Video S1, Supporting Information). In all cases, a thin silicone elastomer ($\approx 25 \mu\text{m}$) encapsulates the system, and a low modulus acrylic adhesive ($\approx 25 \mu\text{m}$) serves as the substrate. The ultraminiaturized, thin, lightweight construction provides wide ranging options for mounting on the human body, including locations where long-term integration is possible and where interfaces to both the body and an external device are easily established.

The fingernails and toenails provide examples. By comparison to the skin, the nails are hard, physically static and they lack sensory capacity, thereby providing a minimally invasive interface for robust, long-term integration with a cyanoacrylate adhesive. The growth cycle from the quick to the end of the nail can exceed 6 months, thereby allowing integration for several months.^[11] Such timeframes greatly exceed those associated with mounting on the skin, where the cycle for skin cell differentiation and exfoliation occurs on the timescale of few weeks. The fingernails of adults have radii of curvature that range from ≈ 13 to ≈ 5 mm,

depending on age, sex, overall body size, and finger.^[12] Properly designed devices can accommodate bending associated with mounting on such surfaces, without significant change in operating characteristics. Figure 2 shows the electromagnetic properties of mm-NFC devices at bending curvatures relevant to the fingernail. These evaluations use the largest device (7.04 mm coil diameter) because this format involves the most significant change at any given curvature. In all cases, resonance frequencies measured by the Min-phase method^[13] match those determined by electromagnetic simulations (Ansys HFSS 13 User's guide, Ansys, Inc. 2011). Typically, the frequencies increase with bending curvature due to decreases in the projected areas and the associated inductances. The magnetic flux through the coil of the mm-NFC device is $\Phi = \iint_S B \times dS$, where B is the magnetic field produced by primary coil and S is the corresponding in-plane area enclosed by the coil of the mm-NFC device. For a large commercial primary coil (Samsung Galaxy Note II), the magnetic field B remains essentially the same when the small mm-NFC devices are bent, such that the magnetic flux Φ depends only on the effective area S of the coil of the mm-NFC device. The change of effective area S is $(d_i/R)^2/32$, where d_i is the inner diameter of the mm-NFC device and R is the radius of curvature. For the mm-NFC device with 7.04 mm outer diameter ($d_i = \approx 5$ mm as in experiments) and $R > 5$ mm for the adult human fingernails, the effective area S only decreases by $\approx 3.1\%$ for $R = 5$ mm. The magnetic flux therefore also remains unchanged when the mm-NFC devices are mounted onto the fingernails, as confirmed by Figure 2a. The resonance frequency can be obtained from $f_{\text{resonant}} = 1/(2\pi\sqrt{L(f_{\text{resonant}}, R)C})$, where C is the capacitance of the NFC die, and the effective inductance L of the coil of the mm-NFC device depends on the frequency f and radius of curvature R as shown in Figure S1 (Supporting Information). The maximum difference between the effective inductance for a planar coil and one with a radius of curvature 5 mm is only $\approx 3\%$ as shown in Figure S1 (Supporting Information). By consequence, the resonance frequencies and the Q factors remain ≈ 14 MHz and ≈ 15 , respectively, for a bending radius $R > \approx 5$ mm. Changes can be observed when R becomes significantly smaller than 5 mm, as shown in Figure 2d,e.

The electromagnetic coupling between a primary coil and an mm-NFC device depends strongly on size, as expected from the expression for magnetic flux. Three mm-NFC devices with different radii given in Table S1 (Supporting Information) are studied, where the number of turns and layers are adjusted to offer the same inductances, i.e., these mm-NFC devices have the same resonant frequency and Q factor as shown in Table S1 (Supporting Information) and return loss spectra as shown in Figure S2a (Supporting Information). As the size of mm-NFC device decreases, the amplitude of phase decreases rapidly as shown in Figure S2b (Supporting Information), which suggests that the communication between the primary coil and mm-NFC device weakens significantly as the coil size of mm-NFC device decreases.

The nature of fingernail growth affords increased mounting times for mm-NFC devices that adopt elliptical shapes with major axes oriented parallel to the base of the nail. Figure 3 shows the results for mm-NFC devices with such shapes and with areas similar to those of circular designs (πR^2), for several different aspect ratios $b/a = 1.21, 1.44, \text{ and } 1.69$, with the major axes a and

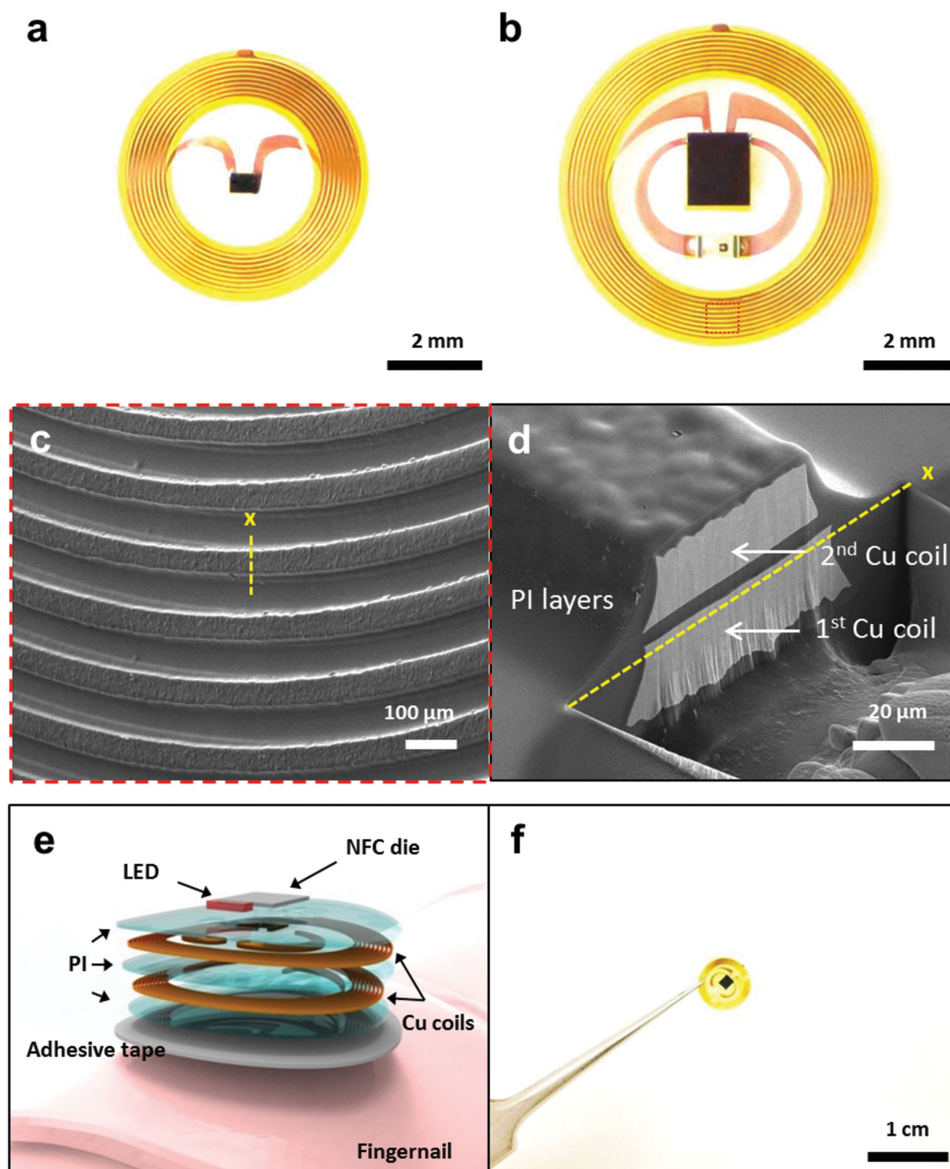


Figure 1. Schematic illustration and images of flexible mm-NFC devices with and without LEDs. a,b) Pictures of the devices and c) scanning electron microscope image of the region of (b) indicated by the red dashed box. d) Cross-sectional SEM image of one part of the coils. e) Exploded-view schematic illustration of each layer of a device mounted on a fingernail. f) Picture of a free-standing device held at one edge by tweezers.

b shown in Figure 3c. The resonance frequency and the amplitude of the phase decrease only slightly as the aspect ratio b/a increases as shown in Figure 3b,c. As a result, the resonance frequencies and the Q factors remain essentially unchanged, i.e., 14 MHz and 15, respectively, for this range of aspect ratio (Figure 3d,e).

Flexible mm-NFC devices also offer advantages for mounting on the skin. Here, the small sizes minimize sensory perception and reduce energy release rates for delamination. Figure 4a shows images of a device with 7.04 mm outer diameter printed onto a low modulus substrate (PDMS, 20 mm length in stretching direction, 25 mm width, 3 mm thick, 0.145 MPa modulus) in various deformed states, including tests that involve stretching to 20% and compressing to 20%, repeatedly. Even after 10 000 cycles, the device shows no form of degradation

in properties (Figure 4c). Figure 4b presents the stress distributions at the interface between the substrate and mm-NFC device obtained from finite element analysis (ABAQUS Analysis User's Manual 2010, V6.10). For both stretching and compressing, the normal stress is negligibly small as compared to the shear stress at the interface; the latter is smaller than the threshold (20 kPa)^[14] for somatosensory perception of forces by normal skin under 20% stretching. For compressing by 20%, which is larger than that expected in most practical applications, the shear stress exceeds the threshold 20 kPa over a small region ($\approx 4 \text{ mm}^2$) of the interface. The energy release rate^[15] for an infinitesimal crack at the edge is $G = \frac{E_{\text{sub}} \epsilon_{\text{app}}^2}{8(1-\nu_{\text{sub}}^2)} L_0 \tan \frac{\pi D}{2L_0}$, where D is the diameter of the mm-NFC device, L_0 is the length

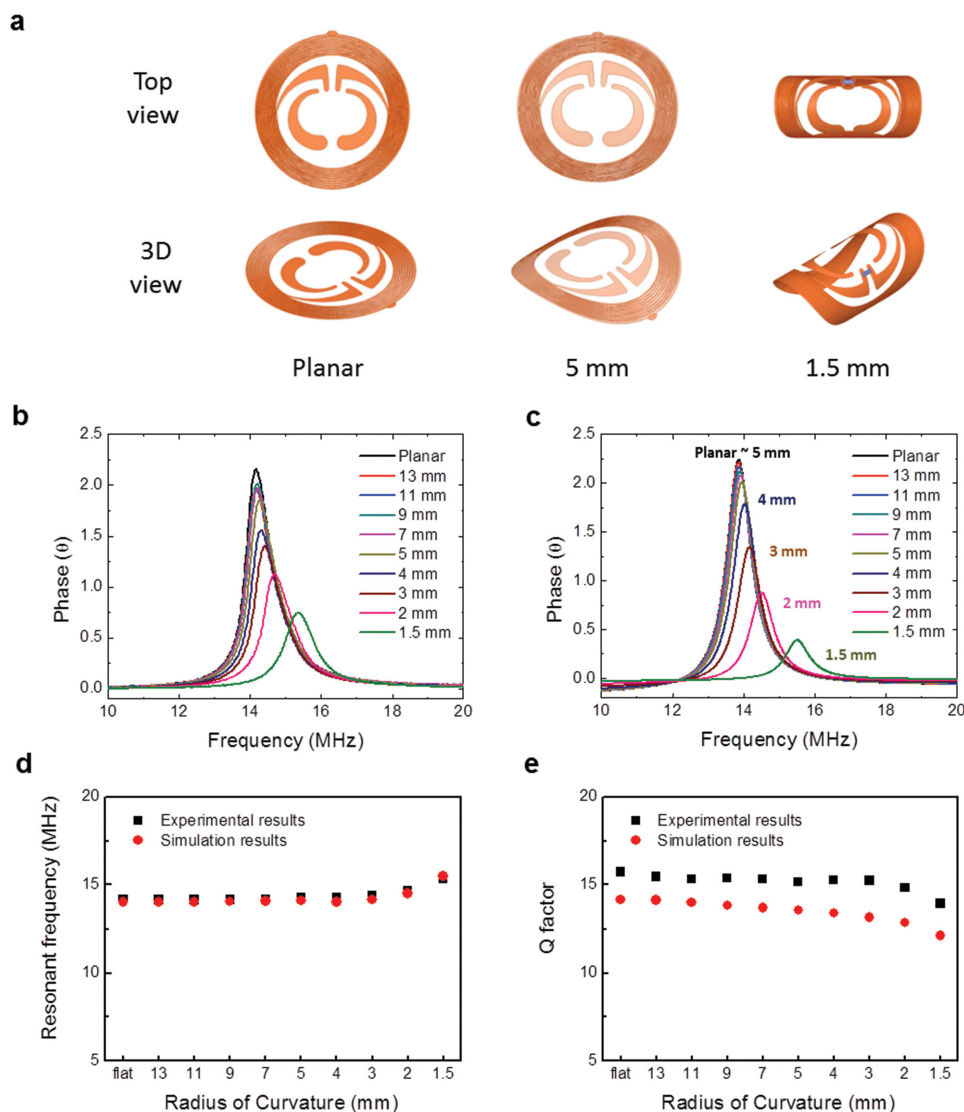


Figure 2. Experimental and simulation results for the electromagnetic properties of flexible mm-NFC devices bent to different radii of curvature. a) Top view and 3D illustrations devices at different curvatures. b) Measured phase responses of the coils as a function of radius of curvature and c) corresponding simulation results. d) Measured and simulated changes in resonant frequency with radius of curvature. e) Measured and simulated changes in Q factor with radius of curvature.

of substrate in the stretching direction, ϵ_{app} is the average strain in the substrate, and E_{sub} and ν_{sub} are the Young's modulus and Poisson's ratio of the substrate, respectively. As shown in Figure 4d, the energy release rate clearly decreases with the coil diameter D , and becomes linear with respect to D for small mm-NFC devices, i.e., $G = \frac{\pi D E_{sub} \epsilon_{app}^2}{16(1 - \nu_{sub}^2)}$. This scaling affords

advantages reduced possibility for delamination of mm-NFC devices from the skin. Figure 4e,f shows the picture of a device mounted on the skin during a pinching mode deformation and the stress distributions at the interface from finite element analysis, respectively. The device is fully bonded with the skin even when the skin is subjected to severe wrinkle. Minimizing the size maximizes the robustness of the device/skin bonding interface for any given adhesive strategy and device construction.

Figure 5 presents images of devices mounted on various locations of the body, each suggestive of a possible application. Figure 5a shows an mm-NFC device on the fingernail such that, for example, natural motions associated with handling the phone could unlock its operation, as shown in Figure 5b. The communication distance of the NFC devices depends on coil size. Figure S4 (Supporting Information) shows the phase responses measured at different distances. Only minor changes in the resonant frequencies and amplitudes of the phase responses occur for distances of up to 17 mm. Communication is possible through the finger and at a distance of ≈ 20 mm with a standard smartphone. This type of authentication could be useful in many contexts (Figure 5c). Multiple devices with different purposes can easily be accommodated in one convenient area (Figure 5d). Certain NFC die (SL13A, ams AG) offer integrated capabilities in temperature sensing and other

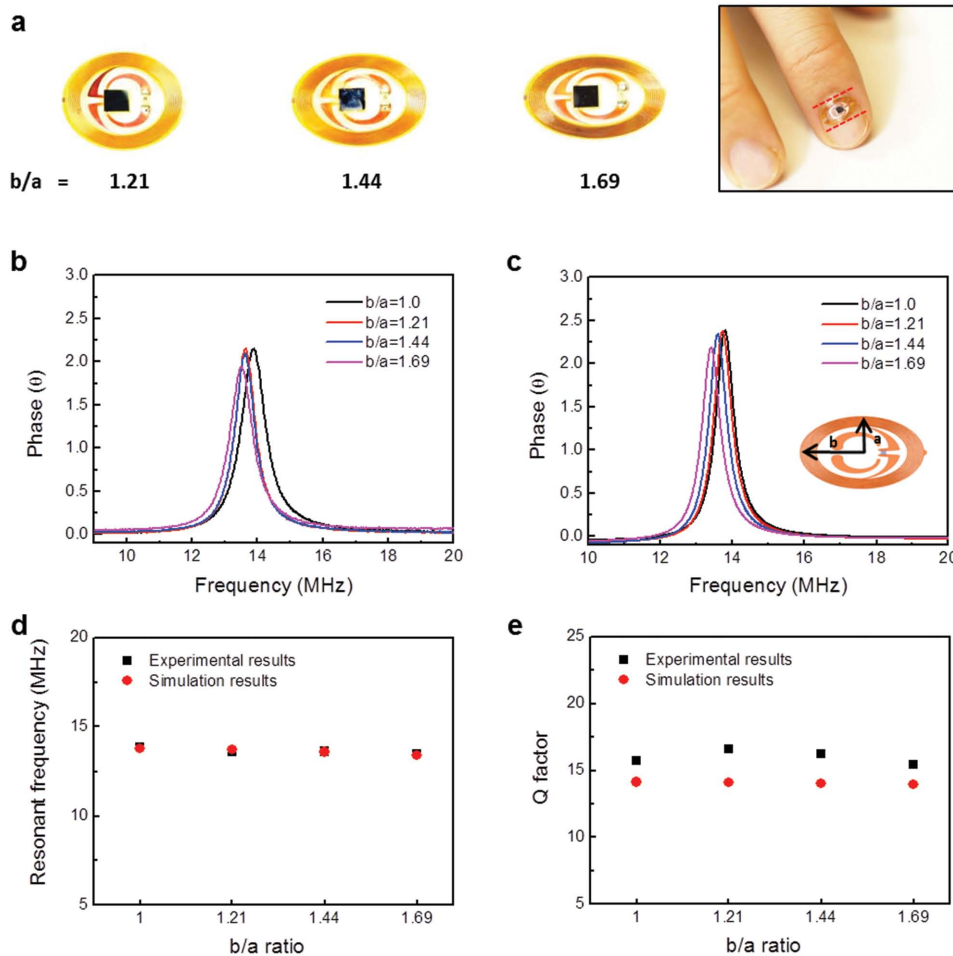


Figure 3. Experimental and simulation results for the electromagnetic properties of mm-NFC devices with elliptical shapes. a) Pictures of elliptical mm-NFC devices with different eccentricities (i.e. ratios of major to minor axes, b/a). b) Measured phase responses of the coils as a function of eccentricity and c) corresponding simulation results. d) Measured and simulated changes in resonant frequency with b/a . e) Measured and simulated changes in Q factor with b/a .

functionality. The inset of Figure 5e shows an mm-NFC device for temperature sensing. In this case, a skin-integrated configuration could be useful (Figure 5e,f). The devices can also function properly on teeth and under water (Figure 5g,h), thereby suggesting modes for chemical sensing in biofluids.

3. Conclusion

The materials, device designs, and integration strategies presented here provide a framework for mm-scale, flexible, body-worn NFC systems, with potential applications in password authentication, electronic transactions, and biometric sensing. The ultraminiaturized geometries and mechanically flexible designs, in particular, afford advantages in mechanical strength, placement versatility, and minimized interfacial stresses. Combined theoretical and experimental considerations in materials, electromagnetic characteristics, and mechanical properties are essential to proper design. These concepts can apply to many other types of wireless communication systems including various biosensors and electronic implants.

4. Experimental Section

Fabrication of the Coils: A Cu foil (18 μm thick, Oak Mitsui Micro-thin series) served as the material for the first coil layer. A layer of polyimide (2.4 μm thick, PI2545, HD Microsystems) spin-cast at 2000 rpm for 30 s, baked on a hot plate at 150 $^{\circ}\text{C}$ for 5 min, and in a vacuum oven at 250 $^{\circ}\text{C}$ for 70 min formed an insulating coating. Laminating this PI-coated Cu foil onto a glass slide coated with polydimethylsiloxane (PDMS, Sylgard 184), with the PI side down, allowed patterning of the Cu into a coil geometry by photolithography (AZ 4620 photoresist, spin-casting at 3000 rpm for 30 s, baking at 110 $^{\circ}\text{C}$ for 3 min, UV irradiance for 300 mJ cm^{-2} , development for ≈ 40 s with developer AZ 400K/deionized water solution of 1:2 volume ratio), and wet etching (CE-100 copper etchant, Transense, etching for ≈ 10 min with frequent rinsing by water). A coating of PI spin-cast at 1000 rpm for 30 s covered the first coil layer. Photolithography (AZ 4620) and oxygen plasma etching created via holes through the PI. Oxide remover (Flux, Worthington) eliminated the native copper oxide at the base of via holes. Electron beam evaporation formed a conducting layer (500 nm thick) for electroplating. Next, electroplating (11 wt% cupric sulfate pentahydrate in water, current of 13 mA cm^{-2} for 55 min, distance between positive electrode and negative electrode of 1.7 cm) generated a second coil in a 20 μm thick layer of Cu, also patterned by photolithography (AZ 4620) and wet etching (copper etchant). Spin casting formed another 2.4 μm

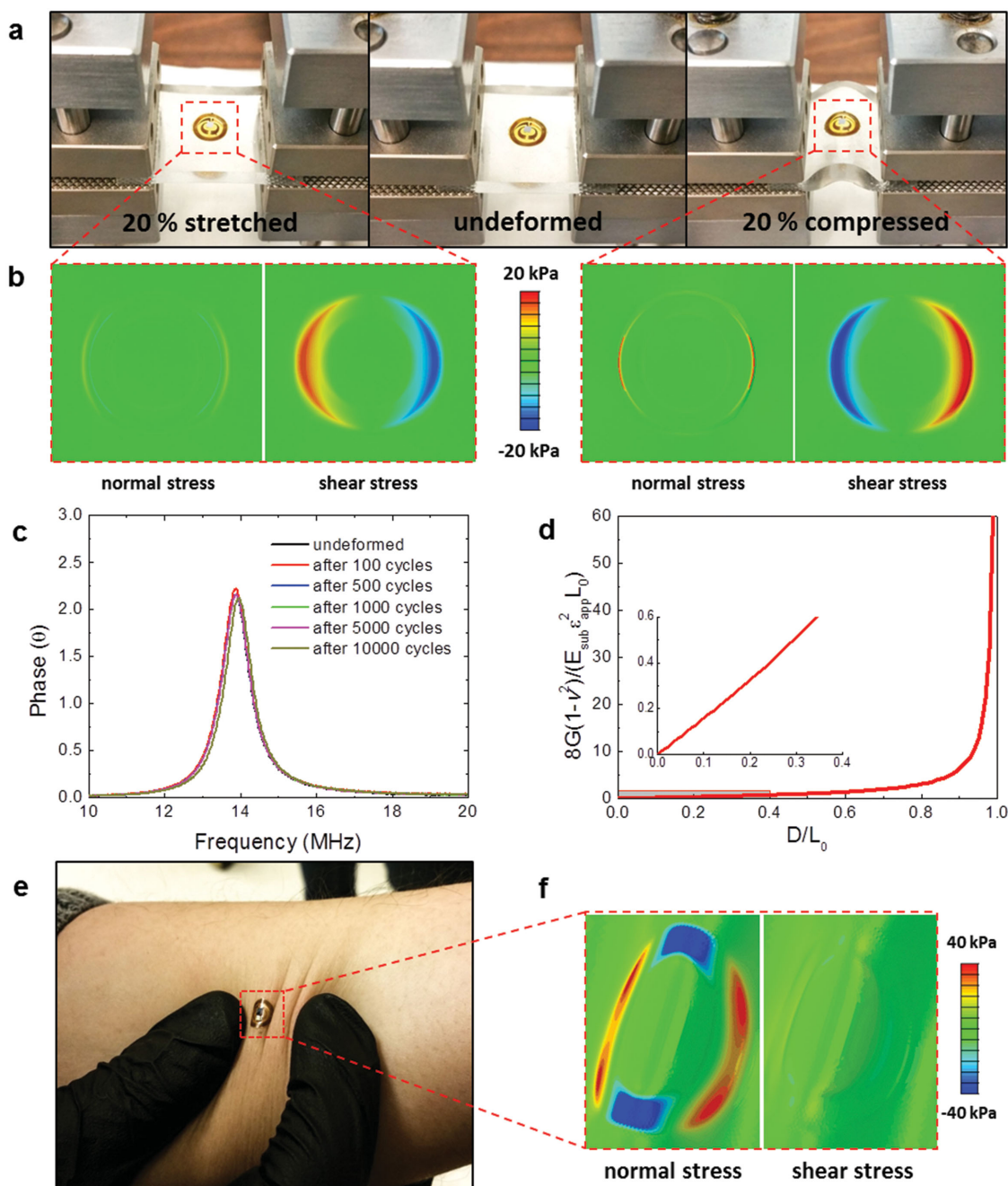


Figure 4. Experimental and simulation results of the mechanical responses of flexible mm-NFC devices to applied strain. a) Pictures of a representative device mounted onto a soft silicon substrate that is undeformed (center), stretched (left), and compressed (right) by application of force using a mechanical stage. b) The bottom frames show corresponding FEA results of applied stresses. c) Phase responses measured after different numbers of cycles of uniaxial stretching (to 20%)/compressing (to 20%). d) Plot of the energy release rate with the diameter of mm-NFC device. e) Picture of a device mounted on the skin during a pinching mode deformation. f) Simulated stress distributions near the device.

thick layer of PI over the entire coil structure. Electron beam evaporation of a 50 nm thick layer of SiO₂ created a hard mask in a geometry defined by photolithography (AZ 4620) and RIE etching (50 mTorr, 40 sccm CF₄, 100 W for 10 min). Oxygen plasma removed the exposed PI, leaving PI only in the regions of the coil, for an open architecture design that improves the mechanical deformability.

NFC Die: The NTAG216 (NXP Semiconductor, ISO/IEC 14443, input capacitance of 50 pF) chip served as the electronics for the smallest device. The M24LR04E (ST Microelectronics, ISO/IEC 15693, input

capacitance of 27.5 pF) chip was used for the energy harvesting device. The SL13A (ams AG, ISO/IEC 15693, input capacitance of 25 pF) chip enabled the temperature sensing device. All chips were thinned (<100 μm thick) and used as bare die without packages.

Transfer and Chips Assembly: A cellulose-based water-soluble tape (Grainger) allowed retrieval of the fabricated coils from the substrate and integration onto an adhesive substrate. Removal of the water-soluble tape by dissolution in water completed the transfer. Thinned NFC die and LEDs attached to the coil by a modified flip-chip bonding method



Figure 5. Pictures of various points of integration of mm-NFC devices on the body, each suggestive of a different application possibility. a) Picture of a device on the fingernail. Pictures of applications to unlock b) a smartphone and c) computer (using a mouse). d) Picture of a set of devices with integrated LEDs mounted on the fingernails. e,f) Pictures of a device mounted on the skin behind the ear, with integrated temperature sensing capabilities. Inset: Picture of a device that enables temperature sensing. Pictures of devices g) on a tooth and h) submerged in water.

with an indium/Ag-based solder paste (Ind. 290, Indium Corporation; ≈ 165 °C for 2 min in a reflow oven). A droplet of silicone elastomer (Q1-4010, Dow Corning) encapsulated the chips.

Electromagnetic Characterization: Electromagnetic characterization used an impedance analyzer (4291A RF impedance/material analyzer, Hewlett Packard) with a commercial primary coil (Samsung Galaxy Note II; resonant frequency ≈ 47.5 MHz) over a frequency range of 5–20 MHz. The Min-phase method defined the resonance frequencies of the NFC devices. Measurements involved placement of the device at the center of the primary coil at a vertical distance of ≈ 2 mm, as shown Figure S3 (Supporting Information).

Supporting Information

Supporting Information is available from the Wiley Online Library or from the author.

Acknowledgements

This work was supported by the Global Research Laboratory (GRL) Program (K20704000003TA050000310) through the National Research Foundation of Korea (NRF) funded by the Ministry of Science, and used facilities in the Frederick Seitz Materials Research Laboratory and the Center for Microanalysis of Materials at the University of Illinois at Urbana-Champaign. Z.X., F.L., and X.F. acknowledge the support from the National Basic Research Program of China (Grant No. 2015CB351900) and National Natural Science Foundation of China (Grant Nos. 11402134, 11320101001). P.G. acknowledges an Australian Government Endeavour International Postgraduate Research Scholarship and the Australian Nanotechnology Network Overseas Travel Fellowship. Y.H. acknowledges the NIH grant and NSF grant.

Received: April 20, 2015

Revised: May 21, 2015

Published online: June 18, 2015

[1] G. B. Raupp, *ECS Trans.* **2011**, *37*, 229.

[2] J. Kim, A. Banks, H. Y. Cheng, Z. Q. Xie, S. Xu, K. I. Jang, J. W. Lee, Z. J. Liu, P. Gutruf, X. Huang, P. H. Wei, F. Liu, K. Li, M. Dalal,

R. Ghaffari, X. Feng, Y. G. Huang, S. Gupta, U. Paik, J. A. Rogers, *Small* **2015**, *11*, 906.

[3] J. Sidén, V. Skerved, J. Gao, S. Forsström, H.-E. Nilsson, T. Kanter, M. Gulliksson, presented at *Proc. 4th Int. Symp. Applied Sciences in Biomedical and Communication Technologies* **2011**.

[4] D. H. Kim, N. S. Lu, R. Ma, Y. S. Kim, R. H. Kim, S. D. Wang, J. Wu, S. M. Won, H. Tao, A. Islam, K. J. Yu, T. I. Kim, R. Chowdhury, M. Ying, L. Z. Xu, M. Li, H. J. Chung, H. Keum, M. McCormick, P. Liu, Y. W. Zhang, F. G. Omenetto, Y. G. Huang, T. Coleman, J. A. Rogers, *Science* **2011**, *333*, 838.

[5] a) S. Xu, Y. H. Zhang, L. Jia, K. E. Mathewson, K. I. Jang, J. Kim, H. R. Fu, X. Huang, P. Chava, R. H. Wang, S. Bhole, L. Z. Wang, Y. J. Na, Y. Guan, M. Flavin, Z. S. Han, Y. G. Huang, J. A. Rogers, *Science* **2014**, *344*, 70; b) J. R. Windmiller, A. J. Bandodkar, G. Valdes-Ramirez, S. Parkhomovsky, A. G. Martinez, J. Wang, *Chem. Commun.* **2012**, *48*, 6794.

[6] a) K. I. Jang, H. U. Chung, S. Xu, C. H. Lee, H. Luan, J. Jeong, H. Cheng, G. T. Kim, S. Y. Han, J. W. Lee, J. Kim, M. Cho, F. Miao, Y. Yang, H. N. Jung, M. Flavin, H. Liu, G. W. Kong, K. J. Yu, S. I. Rhee, J. Chung, B. Kim, J. W. Kwak, M. H. Yun, J. Y. Kim, Y. M. Song, U. Paik, Y. Zhang, Y. Huang, J. A. Rogers, *Nat. Commun.* **2015**, *6*, 6566; b) J. W. Jeong, W. H. Yeo, A. Akhtar, J. J. S. Norton, Y. J. Kwack, S. Li, S. Y. Jung, Y. W. Su, W. Lee, J. Xia, H. Y. Cheng, Y. G. Huang, W. S. Choi, T. Bretl, J. A. Rogers, *Adv. Mater.* **2013**, *25*, 6839.

[7] M. Q. Saeed, C. D. Walter, 2012 in *Int. Conf. Internet Technology and Secured Transactions* **2012**, 730.

[8] M. Fisher, *Blaze Mobile, Inc., US 8352323 B2*, **2013**.

[9] D. P. Rose, M. Ratterman, D. K. Griffin, L. Hou, N. Kelley-Loughnane, R. R. Naik, J. A. Hagen, I. Papautsky, J. Heikenfeld, *IEEE Trans. Biomed. Eng.* **2015**, *62*, 1457.

[10] A. Žnidaršič, B. Werber, in *BLED 2014 Proc., Slovenia* June, **2014**.

[11] W. B. Bean, *Arch. Intern. Med.* **1980**, *140*, 73.

[12] S. Murdan, *Int. J. Cosmetic Sci.* **2011**, *33*, 509.

[13] a) T. J. Harpster, B. Stark, K. Najafi, *Sens. Actuators A* **2002**, *95*, 100; b) X. Huang, Y. H. Liu, H. Y. Cheng, W. J. Shin, J. A. Fan, Z. J. Liu, C. J. Lu, G. W. Kong, K. Chen, D. Patnaik, S. H. Lee, S. Hage-Ali, Y. G. Huang, J. A. Rogers, *Adv. Funct. Mater.* **2014**, *24*, 3846.

[14] S. D. Wang, M. Li, J. Wu, D. H. Kim, N. S. Lu, Y. W. Su, Z. Kang, Y. G. Huang, J. A. Rogers, *J. Appl. Mech. Trans. ASME* **2012**, *79*, 031022.

[15] N. S. Lu, J. I. Yoon, Z. G. Suo, *Int. J. Mater. Res.* **2007**, *98*, 717.